ChemComm

Significance of Thermodynamic Interaction Parameter in Guiding the Optimization of Polymer:Nonfullerene Solar Cells

Journal:	*ChemComm*
Manuscript ID	CC-FEA-07-2020-004869.R1
Article Type:	Feature Article

FEATURE ARTICLE

Significance of Thermodynamic Interaction Parameter in Guiding the Optimization of Polymer:Nonfullerene Solar Cells

Received 00th January 20xx,
Accepted 00th January 20xx

DOI: 10.1039/x0xx00000x

Mengyuan Gao[a], Ziqi Liang[a], Yanhou Geng[a], and Long Ye*[a,b]

Polymer solar cells (PSCs) based on polymer donors and nonfullerene small molecule acceptors are a very attractive technology for solar energy conversion, and their performance are heavily determined by film morphology. It is of considerable interest to reveal instructive morphology-performance relationships of these blends. This Feature Article discusses our recent advances in analysing the morphology formation of nonfullerene PSCs with an effective polymer thermodynamic quantity, *i. e.*, Flory-Huggins interaction parameter χ. In particular, guidelines of high and low χ systems are summarized. The fundamental understanding of χ and its correlations to film morphology and photovoltaic device parameters is of utmost relevance for providing essential materials design criteria, establishing suitable morphology processing guidelines, and thus advancing the practical applications of PSCs based on nonfullerene acceptors.

1. Introduction

Polymer solar cells (PSCs), as a photovoltaic technology with significant potential in modern buildings, greenhouses, indoor and space applications[1-5], have become a research hotspot in the fields of chemistry and material science during the recent years[6, 7]. As the core layer for sunlight to electricity conversion, the active layer of a PSC is generally composed of bulk-heterojunction blends of polymer donors and (polymer or small molecule) acceptors. The continuous improvement of device performance of PSCs is driven by the rapid development of novel donor and acceptor materials. In addition to the molecular structures of photovoltaic materials, film morphology is an important factor that cannot be ignored[8-12]. The final morphology of a PSC film is the result of combined influences of mixing thermodynamics and kinetics during the film solidification process[10].

Of the continually increasing number (>1000) of nonfullerene small molecule acceptors (NFAs), each could be paired with thousands of donor polymers being extensively developed in the past decade. Yet, power conversion efficiencies (PCEs) over 18% are only achievable for very few pairs of materials with finely-tailored properties through extensive explorations[13, 14]. To quickly identify promising donor:acceptor combinations and best processing protocols is still an exhausting process[15-17]. The approach heavily relies on tedious trial-and-error procedures and labour-intensive efforts which are certainly unsustainable. As a good starting point of rational optimization, miscibility is a very important concept widely used for describing the morphology of polymer:fullerene systems, for instance, polythiophene:fullerene systems by various groups[18-23], and low bandgap donor-acceptor copolymer:fullerene blends mostly by the Ade group[24-28] and Chen *et al*.[29]. Despite the miscibility characterizations of polymer:fullerene blends have been well summarized by several perspectives[30-32], the recent progress on mixing thermodynamics of PSC blends based on NFAs has not been overviewed. With the development of new NFAs, relating mixing thermodynamics to morphology and device performance has received increasing attention in recent years. Thus, a thorough survey of the thermodynamic studies of PSCs based on NFAs will be particularly useful to the researchers in this field.

In this Feature Article, we mainly focus on recent efforts in applying Flory-Huggins interaction parameter χ to understand the photovoltaic performance and morphology stability of PSCs, concentrating on polymer:small molecule blend systems (see **Figure 1**). The aim of this article is not to provide a comprehensive review, but a concise overview of the research on interaction parameters of nonfullerene organic photovoltaic blends actively developed in the past five years. The article is divided into five sections. We will start with an introductory overview of interaction parameter χ as described by the Flory-Huggins theory of polymer blends and the common experimental methods used for determining χ (section 2), followed by the relation between χ and morphology derived from scattering principle and lever rule (section 3). Subsequently, we will describe how χ can help understand photovoltaic performance and morphology stability of nonfullerene PSCs by using a variety of representative examples to date. In section 4 and section 5, applications of χ in binary and ternary blend systems based on conjugated polymers and NFAs will be respectively discussed. The interaction parameter between photoactive material and processing solvent and its implications in device processing is discussed in section 6. Finally, we conclude by highlighting the remaining

[a] School of Materials Science and Engineering, Tianjin Key Laboratory of Molecular Optoelectronic Sciences, Tianjin University, Tianjin 30072, China. *Corresponding Author: yelong@tju.edu.cn
[b] State Key Laboratory of Luminescent Materials and Devices, South China University of Technology, Guangzhou 510640, China.

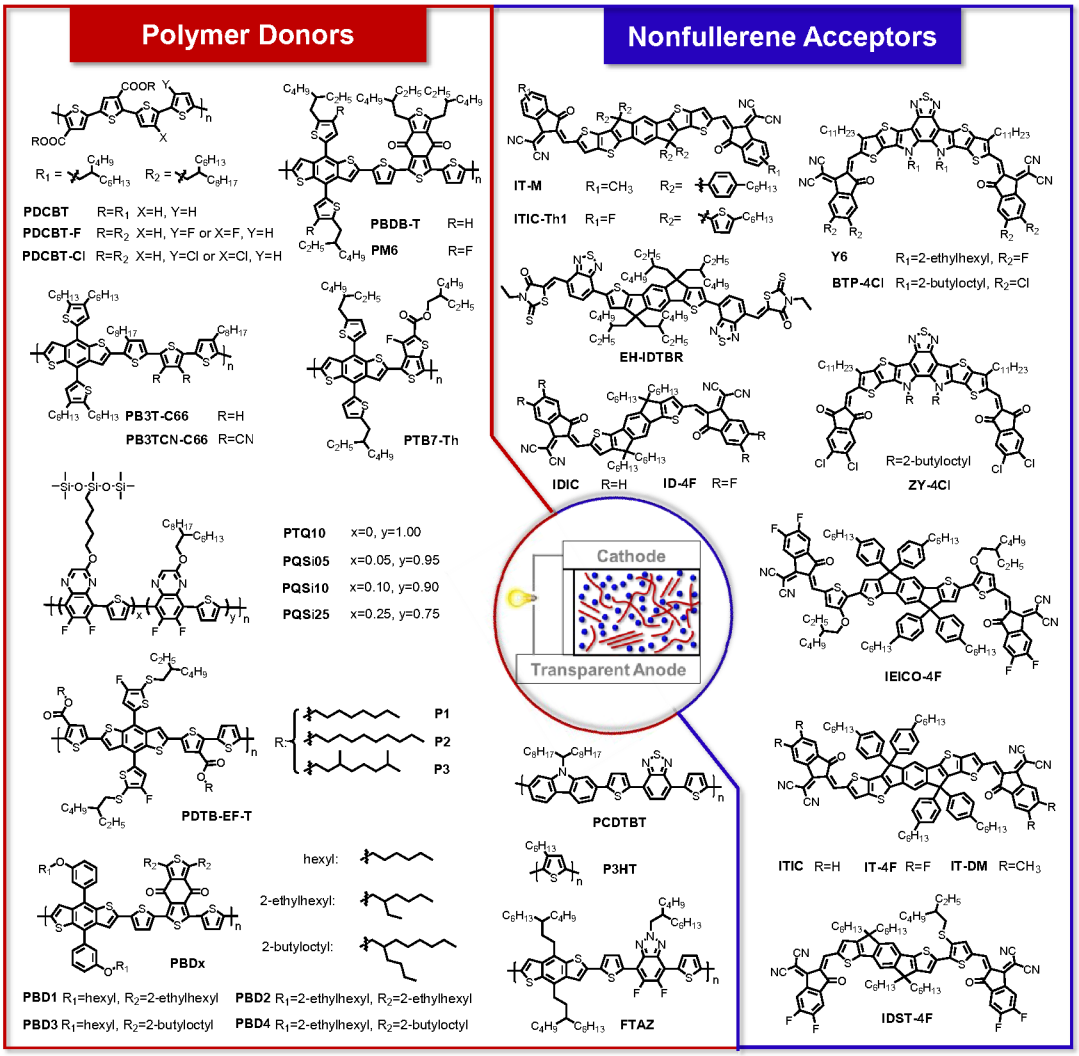

Figure 1. Chemical structures of polymer donors and nonfullerene small molecule acceptors discussed in this Feature Article.

challenges and future opportunities of using χ for conjugated polymer blends.

2. Mixing Thermodynamics of Polymer:Small Molecule Blends

In this section, we will briefly overview the fundamentals of mixing thermodynamics of PSCs from a polymer physics viewpoint and the common experimental methods used for determining χ. We start by overviewing the theoretical background that is relevant to the interaction parameters of polymer blend systems. The phase behaviours of polymer and polymer (or small molecule) blends are described by several theories[33, 34]. Among these, Flory-Huggins solution theory is a very classic and still the most frequently used model[33, 35]. However, the Flory-Huggins theory is only applicable to amorphous mixtures and does not properly consider some potential effects (*e.g.*, local packing, the size differences between blend components, and volume changes during mixing). Despite the possible limitations, this theory is still quite compelling to the PSC researchers and has provided essential (semi-)qualitative insight into the phase behaviours of various conjugated polymer blends and the corresponding polymer solutions[32, 36-46]. According to Flory-Huggins theory, when mixing two solute components labelled "1" and "2" together in a solvent labelled "3", the total change in the Gibbs free energy (G_{mix}) for this ternary system[41] per lattice site is described by the following **Equation 1.**

$$\Delta G_{mix} = kT \left(\frac{\phi_1}{N_1} ln\phi_1 + \frac{\phi_2}{N_2} ln\phi_2 + \phi_3 ln\phi_3 + \chi_{12}\phi_1\phi_2 + \chi_{13}\phi_1\phi_3 + \chi_{23}\phi_2\phi_3\right)$$

(Equation 1)

where ϕ_i represents the volume fraction of each component. The system is assumed to be incompressible by the Flory-Huggins model, so that $\phi_1+\phi_2+\phi_3=1$. N_1 and N_2 represent effective

molecular sizes of components 1 and 2 given in the number of lattice sites, which are related to their degrees of polymerization. k is the Boltzmann constant and T is the absolute temperature in Kelvin. χ_{ij} is the dimensionless binary interaction parameter representing the (enthalpic) interaction between components i and j, also known as Flory-Huggins interaction parameter. This parameter has been the most widely used quantity, characterizing all sorts of polymer-solvent and polymer-polymer interactions. χ_{ij} can be positive, zero, or negative. Lower χ_{ij} indicates the high extent of mixing. During solvent evaporation, the onset of phase separation into the two-phase regime is determined by χ_{12}. **Equation 1** offers a starting point for many equations of interest. For a binary polymer:small molecule blend in the absence of solvent, the total Gibbs free energy of mixing can be reduced to **Equation 2**.

$$\Delta G_{mix} = kT\left(\frac{\phi_1}{N_1} ln\phi_1 + \phi_2 ln\phi_2 + \chi\phi_1\phi_2\right) \textbf{ (Equation 2)}$$

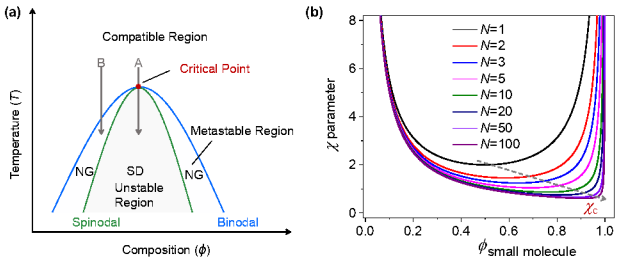

Figure 2. (a) Schematic phase diagram for a polymer blend system illustrating an upper critical solution temperature (UCST) on the temperature-composition plane. The solid line is called the binodal, and the dashed line is the spinodal curve. The binodal curve and spinodal curve meet at a critical point, which also represents the highest temperature of immiscibility. The process of phase separation in the metastable region is the nucleation and growth mechanism (NG), while in the unstable region is the spinodal decomposition mechanism (SD). Arrows A and B indicate the quenching condition. The quench along A is a critical quench (here the system enters the unstable region directly without passing through the metastable region), while that along B is an off-critical quench. (b) Plot of the binodal curves of a polymer:small molecule blend as a function of polymer molecular weight. Here N represents the degree of polymerization of the polymer, which ranges from 1 to 100. The dashed arrow illustrates the change of critical point (χ_c), which is at the apex of the binodal curve.

Figure 2a shows the most commonly observed temperature (T)-composition (ϕ) diagram for a polymer blend. Spinodal and binodal curves are displayed to separate the three regimes (unstable region, metastable region, and compatible region). If one or both of the blend components can crystallize, more complex phase diagrams will emerge[47, 48]. Hereafter we concentrate on a simple yet vitally important case in the PSC field, *i.e.*, polymer:small molecule blend. For each molecular weight, the χ_c is at the lowest point of the binodal curve (as illustrated in **Figure 2b**). The critical interaction parameter χ_c of polymer:small molecule blends can be estimated from **Equation 3**.

$$\chi_c = \frac{1}{2}\left(\frac{1}{\sqrt{N_1}} + 1\right)^2 \textbf{ (Equation 3)}$$

It is clear that χ_c varies from 0.5 to 2.0, which is determined by the degree of polymerization of the polymer donor. χ_c will approach 2.0 if component 1 is a very low molecular weight molecule. In polymer:small molecule blends, increasing the molecular weight of the polymer will result in a more asymmetric binodal with a shift of the critical point towards a higher volume fraction of the small molecule. χ_c is close to 0.5 when the polymer is a very high molecular weight polymer. In the classical sense, χ exhibits a linear reciprocal dependence on T[49] and of course varies for each material combination. Generally, the experimentally observed temperature dependence of χ is described by $\chi(T) = A + \frac{B}{T}$, where A and B are temperature independent constants. A reflects an additional entropic contribution to the combinatorial entropy. If B is positive, increasing T leads to lower χ and higher degree of mixing in a blend; such blends are known as upper critical solution temperature (UCST) systems. On the other hand, negative B value reflects a lower critical solution temperature (LCST) behaviour. In rare cases, an effective $\chi(T)$ describing experimental phase diagrams needs introducing an additional term[50], *i.e.*, C/T^2 or $C\ln(T)$, where C is a constant that is independent on T.

Obviously, the determination of Flory-Huggins interaction parameter χ is the basis and pre-requisite for thermodynamic studies. Experimentally, χ parameters of polymer:small molecule blends can be determined by several methods[32]. Presently, the most commonly used methods to estimate χ are differential scanning calorimetry (DSC) and contact angle measurements. χ might be determined according to the theory of melting point depression[51]. Essentially, the miscibility of the blend system causes the amorphous components to disrupt the arrangement of the crystalline components, which leads to a decrease of melting point. Therefore, the χ parameter of semi-crystalline polymer:small molecule blend system at the melting point can be quantitatively analyzed by using **Equation 4**[43, 51, 52].

$$\frac{1}{T_m} - \frac{1}{T_m^0} = \frac{R}{\Delta H_m}\frac{v_m}{v_s}\left(\phi_s - \chi\phi_s^2\right) \textbf{ (Equation 4)}$$

where T_m^0 and T_m represent the melting temperature of the pure polymer and the blends, respectively. ΔH_m is the melting enthalpy of pure polymer, v_m and v_s identified with the monomer molar volume of polymer and the small molecule, ϕ_s is the volume fraction of the small molecule, and R is the ideal gas constant. As shown in **Equation 4**, the χ parameter can be obtained by fitting the quadratic function of the melting point depression to the volume fraction of small molecules. We recently employed this approach to compare the miscibility of several low-cost polythiophene:nonfullerene blends[53]. Taking the PDCBT-Cl and ITIC-Th1 blend[54] as an example, the DSC curves of pure polymer film and blends with different weight ratios were acquired. As shown in **Figure 3a**, the melting temperature of the polymer decreased gradually with the amount of ITIC-Th1 increasing. Fitting the melting point of pure polymer and blends to **Equation 4** yields χ=0.68 for the PDCBT-Cl:ITIC-Th1 blend system (**Figure 3b**).

Another easily accessible method is contact angle measurement[42, 55, 56]. It can derive the χ parameters of the weakly crystalline or amorphous blend systems, in which melting peaks are absent in the DSC thermograms. The χ parameter could be calculated from the surface energy (γ) by an empirical equation (**Equation 5**).

$$\chi = K\left(\sqrt{\gamma_{polymer}} - \sqrt{\gamma_{small\ molecule}}\right)^2 \text{ (Equation 5)}$$

Where γ is converted by contact angle data and K is a positive constant. Using the contact angle measurement to analyse the miscibility of blend systems has been favoured by many PSC researchers and has been widely used in the miscibility analysis of PSC blends. In a previous study[57], Li *et al.* demonstrated the impact of the intramolecular electron push-pull effect of the NFAs on the miscibility of donor and acceptor by using the measured contact angles of the neat films of PM6, IT-4F and IT-M. The calculation results show that the χ parameter of PM6:IT-4F is higher than PM6:IT-M due to the fact that IT-4F film has larger surface tension than IT-M film. **Figure 3c** provided a non-exhaustive survey of the relative χ values for many PSC systems using contact angle method[54, 57-60].

Temperature-dependent interaction parameter χ(T) can be determined by measuring the device-relevant phase diagrams for the polymer:small molecule blend with time of flight secondary ion mass spectrometry (TOF-SIMS), which tracks the special segments of either polymer or small molecule acceptor using bilayer inter-diffusion approach[61, 62]. χ parameters of the blend system can also be measured by cloud point[63], (X-ray or neutron) scattering[49, 64] reflectivity methods[65] and swelling methods[66]. In addition to the experimental methods, χ parameters can be quickly calculated through the Hansen solubility parameters (HSPs)[67], as given in **Equation 6**. Based upon the group additive approach, HSPs can also be obtained simply based on their molecular structures and molar force data from handbooks[68].

$$\chi = \alpha\frac{V_s}{RT}\left((\delta_{Dp} - \delta_{Ds})^2 + \frac{1}{4}(\delta_{Pp} - \delta_{Ps})^2 + \frac{1}{4}(\delta_{Hp} - \delta_{Hs})^2\right) \text{ (Equation 6)}$$

Where α is the correction term and usually 0.5 in the polymer:small molecule system, V_s is the geometric mean of the molar volume of a polymer with a small molecule, the subscript p identified with the polymer and s with the small molecule, and $\{\boldsymbol{\delta_D}, \boldsymbol{\delta_P}, \boldsymbol{\delta_H}\}$ is the dispersive interactions, polar interactions, and hydrogen bonding interactions, respectively. **Equation 6** might fail in some circumstances[69, 70]. As a complement to the group additive approach, experimental determination of HSPs may be used[71, 72].

3. Bridging Interaction Parameter χ and Film Morphology in PSCs

Before discussing the relation between device function and interaction parameter χ, this section is meant to discuss the role of χ parameter on the morphology of the PSC films. The characterization of film morphology can be performed by the real-space microscopy methods such as transmission electron microscopy (TEM) and atomic force microscopy (AFM) as well as reciprocal-space scattering methods such as resonant soft X-ray scattering (R-SoXS)[73]. Among these, R-SoXS is a favourable technique for quantitative analysis of the characteristic morphology parameters (domain spacing and relative domain purity) of the blend film[74-76]. The long period (L) or centre-to-centre domain spacing is the characteristic length scale of the composition of blend films, it can be calculated by using the equation: $L = 2\pi/q$, where q is the peak location of the scattering maximum.

Domain purity[77] is a vitally important parameter that characterizes the molecular miscibility of the components of the blend films, which can be extracted from the R-SoXS scattering profiles after Lorentz correction, namely $I(q)q^2$ vs q plots. The square root of integrated scattering intensity (*ISI*) over the entire q range of the measurement is used to assess the relative domain purity (σ)[75]. Based on the contrast mechanism of small angle X-ray scattering, the *ISI* of a two-phase system as displayed in **Figure 3d** is expressed as

$$ISI \propto (\phi_2 - \phi_1)^2\varphi_1\varphi_2 \text{ (Equation 7)}$$

where φ_1 and φ_2 are the volume fractions of the two phases, ϕ_1 and ϕ_2 are the concentration of small molecule in the polymer-rich phase 1 and small molecule-rich phase 2. ϕ_0 is the initial volume fraction of small molecule in the blend. Ye and Ade *et al.*[61] derived the mathematical relations between χ and σ based on lever rule ($\phi_0 = \phi_1\varphi_1 + \phi_2\varphi_2$) and **Equation 7**. The readers are directed to the literature[61] for full details of the mathematical derivation. The expression of σ is given by **Equation 8**.

$$\sigma = \sqrt{ISI} \propto \sqrt{(\phi_0 - \phi_1)(\phi_2 - \phi_0)} \text{ (Equation 8)}$$

On this basis, if the thermodynamic equilibrium state is reached, **Equation 9** can be derived as follows

$$\sigma = \sqrt{ISI} \propto \sqrt{(\phi_0 - \phi_{1e})(\phi_{2e} - \phi_0)} \text{ (Equation 9)}$$

where ϕ_{1e} and ϕ_{2e} are the binodal concentrations of small molecules in the two phases. It was clear that both ϕ_{1e} and ϕ_{2e} depend on χ. In general, the composition of polymer in the acceptor-rich phase is almost zero, thus the value of ϕ_{2e} is estimated to be 100 vol%. σ is monotonically related to the acceptor content in mixed phase for a given blend composition ϕ_0. Since χ can be experimentally determined and ϕ_0 is known, ϕ_1 and ϕ_2 at any non-equilibrium states can be inferred from a set of annealing sequence experiments[53, 78]. **Figure 3e** presents an example of increasing *ISI* with annealing time as the mixed domain compositions are evolving from within the two-phase region towards the binodal limit. Usually, optimized device performance was achieved with short annealing (~10 minutes), before the binodal limit was reached[79].

To experimentally verify the above link between χ and phase purity, Ye *et al.*[61] directly measured the device-relevant phase diagrams for a polymer:fullerene blend by TOF-SIMS, which allows

the determination of the temperature-dependent χ for the system. It was found that the obtained (χ, *ISI*) data sets of the model system

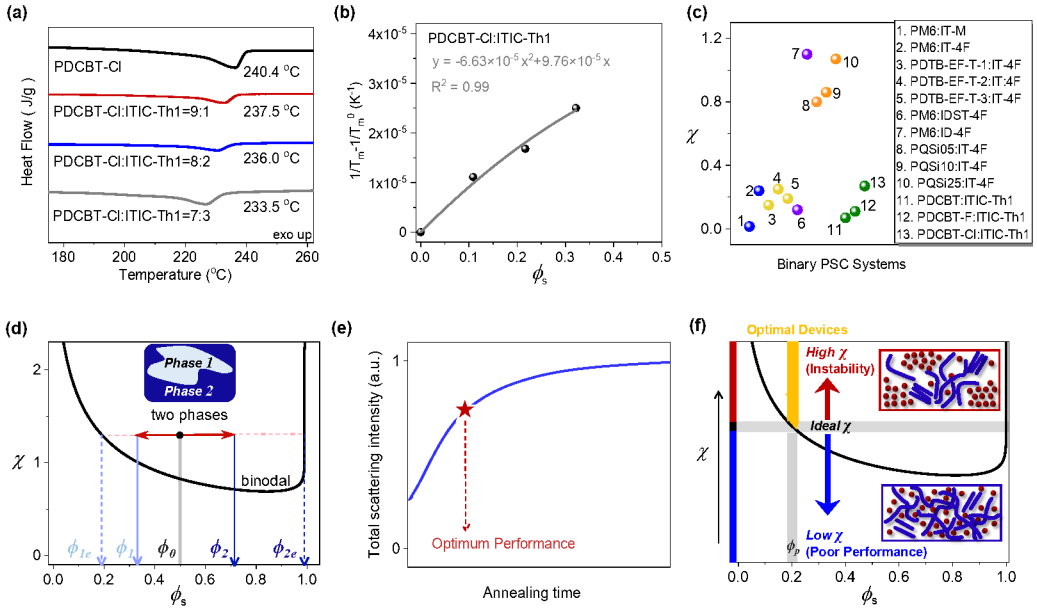

Figure 3. (a) Melting point depression of a polymer:NFA blend (PDCBT-Cl:ITIC-Th1). (b) Fitting the quadratic function of melting point depression and acceptor's volume fraction ϕ_s[53]. Reproduced with permission from ref. 53. Copyright 2020, Elsevier. (c) Plot of the relative χ parameters of over 10 pairs of polymer:NFA blends obtained from surface tension measurements[54, 57-60]. (d) Typical Flory-Huggins theory derived χ-ϕ phase diagram of binary amorphous mixtures of a polymer and a small molecule, which exhibits UCST phase behaviour. Arrows mark the compositions of two phases (1 and 2) in a quenched morphology. Dash lines indicate the binodal compositions. (e) Plot of integrated scattering intensity (*ISI*) as a function of (thermal/solvent vapour) annealing time. The star shows the *ISI* corresponding to the optimum performance of a high χ system. (f) Classification of high χ and low χ regimes (separated by the ideal χ region) in the χ-ϕ phase diagram. The schematic morphology of high and low χ systems are shown as the inset images[32]. Reproduced with permission from ref. 32. Copyright 2018, John Wiley and Sons.

match with the model prediction of **Equation 9**. Further verification was completed with over 10 pairs of high and low performance materials systems. Consequently, these results allow establishing the first model[61] to quantitatively connect thermodynamic χ to phase purity of binary PSC devices.

Based on the literature survey of a wide range of PSC blends[32], it was proposed that three regimes (low χ, ideal χ, and high χ) can be classified by the relation between miscibility and percolation threshold in the context of χ-ϕ phase diagram (**Figure 3f**). In principle, the blend components in the low χ (hyper-miscibility) system tend to be miscible, resulting in less pure domains, which increase the charge recombination and decrease the charge collection efficiency[80]. However, high χ (hypo-miscibility) system has the tendency of spontaneous phase separation, implying that higher phase purity is probably achieved in this case. It generally needs to be quenched to the percolation threshold, where the charge transport is more favourable. Only when the two components are moderately mixed, desirable morphology can be realized. For ideal χ cases, the mixed phase of the blend system possesses a composition near the percolation threshold and stable morphology in the thermodynamic equilibrium state. Since there is only one system exhibiting such an ideal χ[61], nearly all kinds of polymer:NFA blends can be treated as either high χ or low χ systems. We will discuss the χ-performance/stability relationships in low χ and high χ systems in Section 4.

4. Role of Interaction Parameter χ in Binary Blend Systems

The section 4 will introduce how to use the interaction parameters to guide the performance optimization of PSC devices based on polymer:NFA binary blends. While this section cannot cover all of the types of PSC blends known in the literature, we thus use the two most widely used classes of photovoltaic polymers (polythiophenes and benzodithiophene-based copolymers) to highlight the χ-performance relations.

4.1 Guidelines for low χ systems

According to section 3, the relationships between miscibility and the morphology characteristic parameters of PSC films were clarified. Recent experimental studies observed a (mostly) linear correlation between device fill factor (*FF*) and σ.[81, 82] Based on this linear correlation and **Equations 8** and **9**, Ye and Ade *et al.* established the relationship between miscibility and device performance[61]. By investigating a prototypical PSC system

consisting, PCDTBT:PCBM and basing on lever rule and mathematical derivations, a quantitative model between the

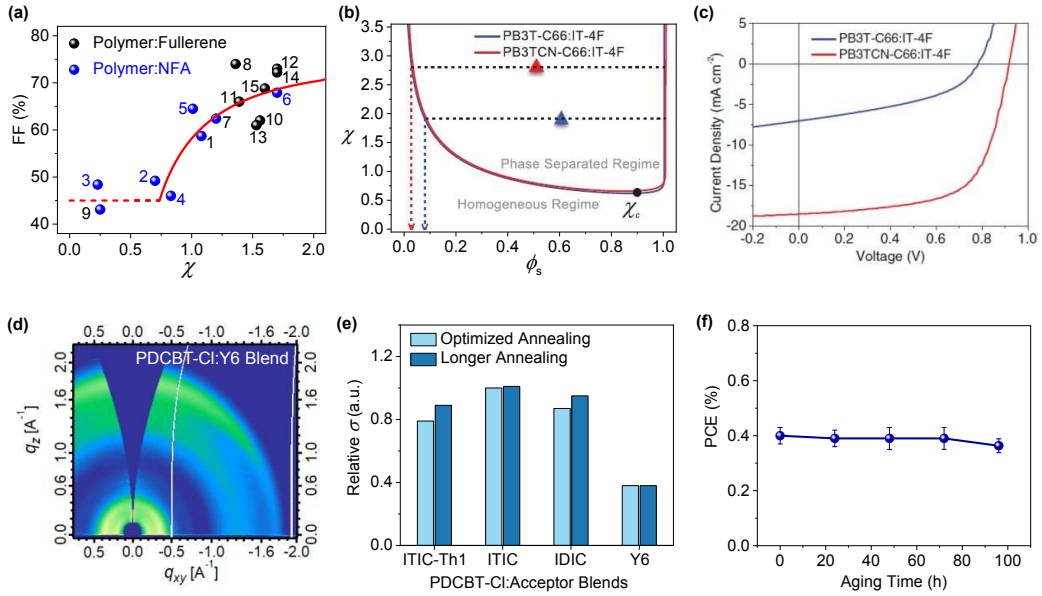

Figure 4. (a) Plot of χ with device fill factor for a wide range of polymer:fullerene and polymer:NFA blends[61]. Reprinted with permission from ref. 61. Copyright 2018, Springer Nature. (b) Illustration of χ-ϕ phase diagram of the PB3T-C66:IT-4F and PB3TCN-C66:IT-4F blends[83]. The solid curves are binodal (coexistence) curves; the horizontal dash lines are the relative χ parameter calculated by HSP, and the vertical dash lines are the maximum IT-4F component in the mixed phases. (c) *J-V* curves of PB3T-C66:IT-4F and PB3TCN-C66:IT-4F[83]. Reprinted with permission from ref. 83. Copyright 2020, John Wiley and Sons. (d) Two-dimensional GIWAXS pattern for PDCBT-Cl:Y6 blend film. (e) Plots of relative composition of PDCBT-Cl:acceptor blends with optimized annealing (2 min) and longer annealing (1 h). (f) Plot of PCE for PDCBT-Cl:Y6 blend as a function of aging time[53]. Reproduced with permission from ref. 53. Copyright 2020, Elsevier.

material-specific interaction parameter χ and device *FF* was then established. Subsequently, the quantitative relationship was established on a variety of polymer:fullerene and polymer:small molecule systems (**Figure 4a**). In this study, the interaction parameter χ has been observed as a critical parameter that impacts bimolecular recombination, and thus the *FF* of PSC devices. The device *FF* increases with increasing χ parameter, that is, the high χ system is easier to achieve high device performance. According to this relationship, researchers can bypass the trial-and-error strategies to guide the selection of donor/acceptor materials, and achieve the performance improvement of devices through reasonable molecular structure modification and morphology optimization methods, especially in low χ systems.

For the hyper-miscibility system, reducing the miscibility of the two components is conducive to the improvement of phase purity, achieving higher device efficiency. For instance, Duan *et al.*[83] introduced cyano group into the polymer PB3T-C66 to alter low χ of PB3T-C66:IT-4F, we compared the miscibility of the two polymers, PB3T-C66 and PB3TCN-C66, with IT-4F by the HSP method (as shown in **Figure 4b**). The results demonstrated that the miscibility of the low χ system is significantly reduced by introducing cyano group into PB3T-C66, resulting in a higher χ for the blend system. Accordingly, the volume fraction of amorphous mixed phases was reduced, combined with the increased domain purity from 0.62 to 1. The optimized phase separation morphology is beneficial to exciton dissociation and inhibits charge recombination along with the improvement of the charge transport. As a consequence, the optimized charge creation and transport facilitate the improvement of J_{sc} and *FF*, achieving a significant increase in PCE from 2.3% to 11.2% (see **Figure 4c**). In addition, In order to reduce the miscibility of the P3HT:BTP-4Cl system, Hou *et al.*[84] designed and synthesized a new acceptor named ZY-4Cl (the chemical structures are shown in **Figure 1**). The P3HT:ZY-4Cl system has a higher χ parameter, driving the appropriate phase separation of the system, which is consistent with the AFM morphology results. Another illustrative example is a comparative study of two PBDB-T:NFA systems[85], namely PBDB-T:IT-M and PBDB-T:IT-DM, which are processed at various processing conditions (as cast, add solvent additive, use both solvent additive and thermal annealing). R-SoXS experiments show that the performance metrics of both device characteristics (J_{sc} and *FF*) increase with the relative average purity. Also, the PBDB-T:IT-M blend films with a higher χ parameter exhibit a larger average purity under various processing conditions, which eventually leads to the increased *FF* and J_{sc}.

We recently discovered that the star acceptor Y6 delivers an abysmal performance with PCE of 0.5% when blended with PDCBT-Cl, although this binary blend shows a rather broad photoresponse range[53]. Grazing incidence wide-angle X-ray scattering (GIWAXS) data shows that the blend is poorly ordered (**Figure 4d**). The DSC and contact angle results display that the PDCBT-Cl:Y6 system is

difficult to phase separate due to its high miscibility, resulting in serious charge recombination and poor device efficiency of only

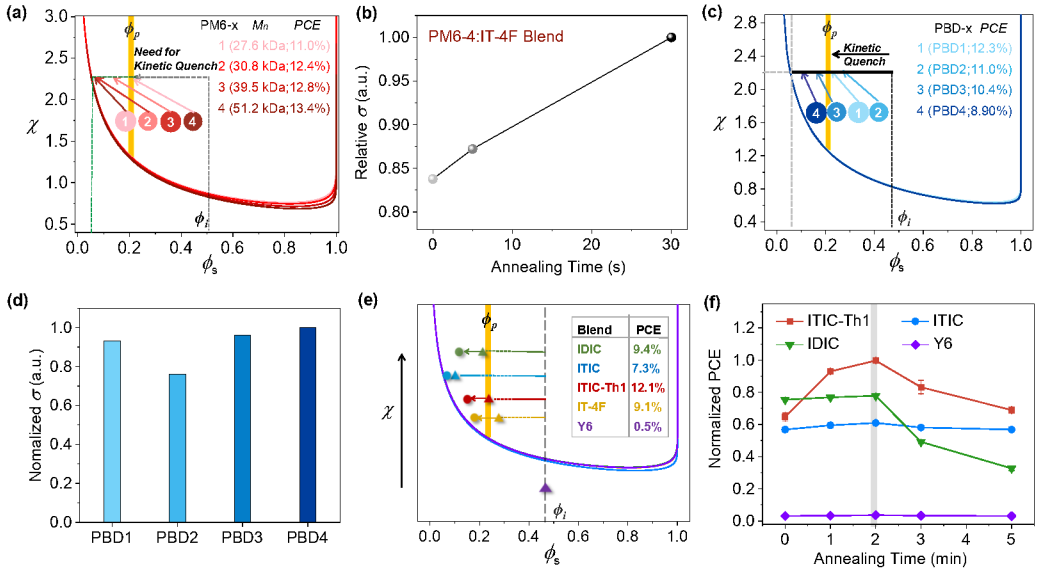

Figure 5. (a) Schematic illustration of the χ-ϕ diagram based on high χ system PM6:IT-4F blends. The polymer M_n values and device PCEs of PM6-x are listed in the diagram. (b) Plot of normalized phase purity (σ) of the highest M_n blend as a function of solvent annealing time[78]. Reproduced with permission from ref. 78. Copyright 2019, Elsevier. (c) Schematic illustration of the χ-ϕ diagram of PBDx:IDIC blends with the variation of polymer side-chain structure. (d) Plot of normalized phase purity (σ) of the IDIC distribution in the mixed phase of the PBDx:IDIC blends[86]. Reproduced with permission from ref. 86. Copyright 2019, American Chemical Society. (e) Schematic illustration of the χ-ϕ diagram based on PDCBT-Cl:NFA blends. Triangles represent the states in optimized devices while dots represent the states in long-time annealed devices. The relative location of the various triangles or dots represent the χ_{aa} of different systems. The best device performance for each blend is depicted in the inset table. (f) Plot of normalized PCEs for four PDCBT-Cl:NFA blends as a function of solvent vapour annealing time[53]. Reprinted with permission from ref. 53. Copyright 2020, Elsevier.

0.5%. Y6 and PDCBT-Cl remained in a homogeneous state due to the hyper-miscibility (χ=0.19) of the two components, which induced impure domains and poor molecular packing in the blend film. **Figure 4e** shows that for the PDCBT-Cl:Y6 blend system, the domain purity is almost the same after solvent vapour annealing for 1 hour. In addition, the devices based on the two photoactive materials exhibit excellent stability, with no significant decrease in device efficiency after long-time aging (see **Figure 4f**). This finding is also in line with the in-operando study on three PTB7-Th:NFA blends by Yip *et al.*[87]. They observed that the lowest χ blend demonstrates the best stability.

4.2 Guidelines for high χ systems

Having discussed the low χ systems, we now turn our attention to high χ systems, *i.e.*, those with hypo-miscibility. It has been previously demonstrated that the acceptor concentration in the polymer-rich mixed domains has to be at or above the electron percolation threshold in order to avoid geminate recombination and facilitate charge extraction[32, 78, 79, 88]. The ability to reach such a concentration depends on miscibility and casting kinetics. In other words, to realize high performance, the morphology often needs to be frozen to a non-equilibrium state, where the acceptor concentration in the polymer-rich mixed phase is suggested to approach the electron percolation threshold to obtain an optimized device performance[88].

A well-studied polymer:NFA system exhibiting high χ is PM6:IT-4F[57, 89]. In 2019, Ye *et al.* selected this high χ system as the model system to examine the effect of kinetic quenching on the morphology and performance[78]. As shown in **Figure 5a**, four batches of PM6 (denoted as PM6-x, x=1-4) with molecular weight varying from 27.6 kg/mol to 51.2 kg/mol were employed. Ye *et al.* utilized TOF-SIMS and hard/soft X-ray scattering to determine the equilibrium composition, quench depth, molecular packing/aggregation, phase separation domain spacing and phase purity of the PM6-x:IT-4F systems. The results showed that the four systems have different PCEs though they display the same χ parameter. Among them, the highest molecular weight devices obtained the highest performance with an efficiency of over 13%, indicating that the phase evolution is not dramatically influenced by thermodynamics but by film-solidification kinetics. Furthermore, the volume fraction of IT-4F in the mixed amorphous phase (7%) was far below the percolation threshold (ϕ_p) of the system (25%), which infers that the mixed phase is excessive purity and needs to be quenched to the ϕ_p for optimized device performance. To further corroborate this viewpoint, the phase purity (σ) of the optimized PM6-4:IT-4F film were analysed as a function of solvent

annealing time through R-SoXS, as provided in **Figure 5b**. It can be seen that with the lengthening of the solvent annealing time, the phase purity of the blend film increases gradually, that is, the acceptor composition of the blends evolves from the quenched state at ϕ_p toward the thermodynamic equilibrium state. These results highlighted that the morphology of the optimized film for high χ systems is indeed kinetically quenched to near the percolation threshold.

Side chain engineering[86] of PBDx (x=1-4, molecular structures are shown in **Figure 1**) also corroborated the above argument. By varying the alkyl chains attached to the donor and acceptor units, Ye *et al.* used the combinations of PBDx and the non-fullerene acceptor IDIC to establish the side chain structure-device performance relations. The length of the alkyl side chain affects the solubility of the polymer in the solution, resulting in different morphological characteristics during the film-formation process. As illustrated in the χ-ϕ phase diagram (**Figure 5c**), all four systems have similar χ parameters yet quite different PCEs, which is related to the fact that the different degree of morphology formation kinetics quenching of the films. Because the PBD1 with the shortest alkyl side chain exhibited the strongest aggregation feature compared with the blends of other polymers PBD2-4, PBD1:IDIC film was kinetically quenched with an acceptor composition close to the ϕ_p, leading to the appropriate phase purity σ of the mixed phase (as displayed in **Figure 5d**) and optimized device performance (PCE over 12%).

The need of optimally kinetic quenching is further validated in the record-efficiency polythiophene:NFA system, PDCBT-Cl:ITIC-Th1[53]. As shown in **Figure 5e**, the blend system achieved over 12% device efficiency due to the appropriate miscibility between donor and acceptor (χ=0.68 by DSC measurement) and the careful control of the mixed phase composition through post-treatment. As presented in **Figure 5f**, after a short period (2 minutes) of solvent annealing, the PCE of the film reached a maximum, and gradually decreased as the solvent annealing time continued to increase. This phenomenon implies that after solvent annealing for 2 min, the blend film of PDCBT-Cl:ITIC-Th1 is locked at the composition near the ϕ_p, where the condition is conducive to promote the efficient charge transport and obtain the optimal performance. Compared with PDCBT-Cl:ITIC-Th1, the PDCBT-Cl:IDIC and PDCBT-Cl:ITIC systems have even higher χ, where the acceptor concentration of mixed domains is difficult to be properly quenched to the ϕ_p and therefore over-purified domains are formed. The oversized phase separation and over-purified domains in the blend films are unfavourable for exciton diffusion and charge transport, resulting in the relatively poor values of J_{sc} and *FF* in the OPVs.

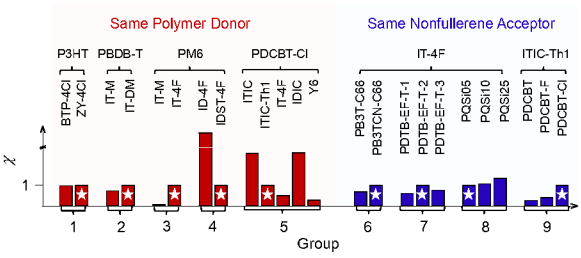

Figure 6. Correlation of chemical structure with the relative interaction parameters of the blends as discussed above. Note that we normalize the χ parameter of the systems to the highest efficiency system to 1 in each group and the highest-efficiency system in each group was marked with a star.

To summarize, the chemical structures of donor and acceptor materials have profound influence on the interaction parameter χ of the blend systems, as shown in **Figure 6.** Note that we normalize the χ parameters of the systems to that of the best-performance system in each group to 1. There exist some empirical rules in molecular design according to multiple case studies. For polythiophene donors, Liang *et al.*[53] reported that the χ_{aa}=1.73, 0.68, and 0.34 for PDCBT-Cl blending with ITIC, ITIC-Th1, and IT4F, respectively. It can be seen that the introduction of F atoms into NFA, the systems exhibit enhanced miscibility with PDCBT-Cl. While for star donor-acceptor type polymer donors (*e.g.,* PM6), Li *et al.*[57] demonstrated that F atoms, which are more electron-withdrawing than methyl, were introduced into the end group of the acceptor, resulting in a lower miscibility than IT-M when blended with PM6.

In high χ systems, the composition of blend film tends to move toward the thermodynamic equilibrium state (binodal composition) during storage, which leads to an acceptor composition of the mixed domain that is much lower than the percolation threshold. This will cause the device performance to degrade rapidly. In a system containing crystalline components, when the thermodynamic equilibrium state is reached, the crystalline components tend to crystallize, leading to further purification of the mixing domain and away from the percolation threshold[62]. However, enhancing the morphology stability of PSC devices is important to guarantee the long-term operation[90]. N. Stingelin and co-workers[37] emphasized that the delicate balance of phase compositions is required for optimal device performance. They highlighted that the vitrification process is of paramount importance, which can dominate the microstructure formation of crystalline blends cast from solution. For example, Ade and co-workers[62] observed strong burn-in degradation in the system of P3HT:EH-IDTBR after annealing at 120 °C for 10 min, which is due to the phase composition far away from the equilibrium state and the crystallization of both P3HT and EH-IDTBR. In contrast, PTB7-Th:EH-IDTBR[91] did not show any small molecule crystalline features and displays superior stability under longer annealing. This is because the glass transition temperature of PTB7-Th is significantly higher than that of P3HT, which leads to a more vitrified system and suppresses the crystallization of small molecules.

It is obvious that the high χ systems cannot achieve high device performance without kinetic quenching the acceptor component of the mixed domain to the percolation threshold, but it is often accompanied by poor device stability due to the evolution of non-equilibrium morphology. However, the vitrification of polymers and small molecules plays a major role in determining the stability in PSC devices and cannot be over-looked. The high degree of vitrification can inhibit burn-in degradation and attain high device stability. By taking the amorphous miscibility of thermodynamics and the kinetic vitrification into consideration, the optimized device performance and higher stability can be obtained simultaneously.

Except for affecting the lateral phase separation, the thermodynamic χ parameter also has a significant effect on the vertical phase separation in the active layer[40, 92, 93], and thus affects the selection of proper device configuration. Contact angle measurement and X-ray photoelectron spectroscopy (XPS) are usually used to characterize the vertical phase separation distribution of the blends. Herein, the study by Li *et al.*[59] was used as an illustration. They employed χ to analyse the vertical phase separation in the case of PDTB-EF-T:IT-4F blend system. Side-chain of the PDTB-EF-T polymer was varied (molecular structures are drawn in **Figure 1**, named P1-3). The vertical phase separation in the active layer shows a strong tendency to occur which can be ascribed to the large difference in surface tensions between P2 (with a linear decyl)

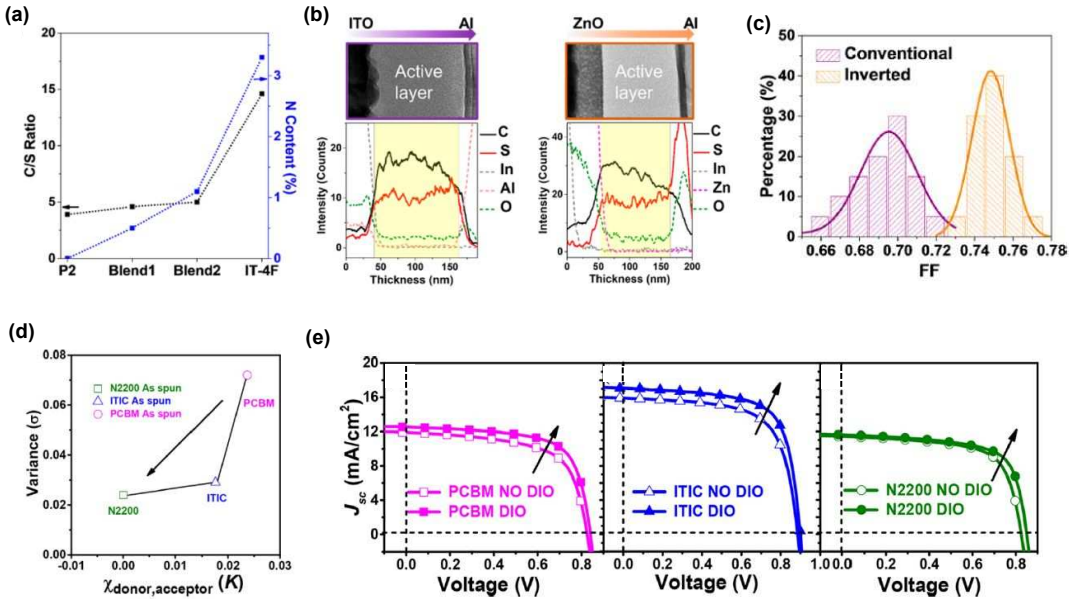

Figure 7. (a) Statistics and Gaussian fitting of the *FF* distribution of the conventional and inverted PSC devices based on P2:IT-4F. (b) Plot of C/S ratios and N contents (%) for the neat films and P2:IT-4F blends obtained via XPS. Blend 1 denotes the P2:IT-4F blend cast on PEDOT:PSS and Blend 2 represent the P2:IT-4F blend cast on ZnO. (c) Cross-sectional TEM images and EDS profiles for the conventional and inverted devices based on the P2:IT-4F blend[59]. Reprinted with permission from ref. 59. Copyright 2018, American Chemical Society. (d) Characteristic *J-V* curves of PBDB-T:PCBM, PBDB-T:ITIC and PBDB-T:N2200 processed with and without DIO. (e) Plot of standard deviations of the acceptor composition in the vertical direction across the PBDB-T:acceptor blends with their χ parameters[94]. Reprinted with permission from ref. 93. Copyright 2019, American Chemical Society.

and IT-4F, corresponding to a higher χ parameter. As can be seen from the XPS, energy dispersive spectroscopy (EDS) and TEM results in **Figure 7a** and **7b**, P2 accumulated near the top electrodes and the IT-4F-rich layer was near the bottom substrates, which experimentally proved the vertical phase separation of the blend system. Due to the high χ, the P2:IT-4F blend film has higher phase purity and favourable vertical phase separation morphology, leading to a *FF* up to 76% (see **Figure 7c**) and a high PCE of 14.2% in the inverted device.

A recent study by Liu and Huang *et al.*[94] also examined the influence of χ parameter on the vertical phase separation of the blends. By measuring the contact angle of neat films, the interaction parameters χ of three different systems are obtained, including $\chi_{PBDB\text{-}T:PCBM}=2.4\times10^{-2}K$, $\chi_{PBDB\text{-}T:ITIC}=1.8\times10^{-2}K$ and $\chi_{PBDB\text{-}T:N2200}=2.9\times10^{-5}K$. The standard deviations (σ) of the acceptor vertical distribution are depicted in **Figure 7d**. Due to the high miscibility of PBDB-T and N2200, there is no obvious phase separation in the vertical direction of the blend film, which makes it difficult to effectively transfer the charge to electrode, resulting in a lower J_{sc} (**Figure 7e**). However, the σ of the vertical distribution of PBDB-T:PCBM system is very large. This is due to the immiscibility between the two components, resulting in the inability to form efficient charge transport pathways. In the PBDB-T:ITIC system, the moderate χ parameter is conducive to the formation of appropriate vertical phase separation, the J_{sc} of this system is up to 16.3 mA cm^{-2}. Besides, the addition of 1,8-diiodooctane (DIO) can further optimize the distribution of the film in vertical direction and in turn improve the efficiency of the inverted device[95]. Understanding the

relationship between interaction parameter χ and phase separation in both lateral and vertical can provide more complete guidance for improving device performance of high χ systems.

5. Role of Interaction Parameter χ in Ternary Blend Systems

For further improving the device performance, ternary blends have been recognized as a potential way cause of the availability to broaden the spectral absorption for the current generation, combined with the simplicity of device architecture[96, 97]. But it is still a long way to establish general design rules for the fabrication of high-efficiency ternary devices. There are generally three types of highly efficient ternary PSCs: polymer:polymer:NFA[98], polymer: fullerene:NFA[99-102], and polymer:NFA:NFA[103, 104]. As the morphology control is typically more complicated and difficult than that of binary blends[105], the screening of a suitable third component still requires a trial-and-error method in most cases. Profit from the development of thermodynamics analysis of the morphology regulation in binary systems, the evaluation of the interaction parameters is also conductive for understanding the complex morphology of ternary blend systems. In this section, we are going to delineate the role of χ in various ternary blends and provide optimization guidelines for device fabrication by using several case studies.

The corresponding guidelines on the selection of an appropriate third component for morphology optimization of high-efficiency devices are preliminarily established through miscibility matching[106, 107]. A typical example of employing the χ of components to help adjust the phase separation in ternary devices was done by Chen and co-workers[98]. In their study, PDCBT served as a third component to the PBDB-T:ITIC binary blend. A negative of χ value (-0.08) for the PBDB-T:PDCBT blend manifests hyper-miscibility between two components. Conversely, PDCBT and ITIC are less miscible with a higher χ value compared with the PBDB-T:ITIC blend. Due to the high crystallinity of PDCBT and hyper-miscibility with PBDB-T, the molecular ordering of PBDB-T is enhanced with the presence of PDCBT, which may act as a nucleating agent. The hypo-miscibility of PDCBT and ITIC eventually leads to the increase of phase domain size and an apparent phase-separated morphology is noticed in ternary films. Ascribed to the enhancement of ordering of polymer stacking and the formation of proper phase separation, the PCE value increases from 9.4% to ~11% in ternary devices.

As we discussed above, for binary blends, the amorphous miscibility needs to be large enough to form an apparent phase separation for the acquisition of high *FF* and thus high PCE values. Therefore, the morphology is generally deeply quenched inside the binodal to form sufficient percolation pathways for the electrons. For these kinds of systems, the poor stability of performance mainly refers to the morphology instability that is primarily driven by thermodynamics, which is even occurred while even storing devices in a dark and inert environment at room temperature. Generally, there are two ways to improve the long-term stability of high χ PSCs. One is to "freeze" the mixed phase in the quenched morphology of high χ systems through using the components with low flexibility and enhancing the vitrification effect. This method was also extensively discussed in section 4. And the other is to introduce the third component which has an appropriate miscibility with the donor polymer at or above the percolation threshold to the initial high χ systems, thereby providing sufficient charge transfer channels to suppress the device degradation[108, 109]. One of our recent studies demonstrated the possibility of suppressing the degradation process for binary systems which include a semi-crystalline acceptor[110]. The blend of PTB7-Th and IEICO-4F is a prototypical system used for semi-transparent and tandem device applications with a remarkable J_{sc} of over 27 mA cm^{-2} and an acceptable PCE of ~11%[111]. However, the binary blends exhibit a pronounced performance degradation for about 35% after shelf aging in darkness for 90 days (**Figure 8a**) demonstrated by Zhu *et al*.[110] The origin of rapid performance degradation can be ascribed to the following reasons. The hypo-miscibility of IEICO-4F and PTB7-Th (measured by TOF-SIMS) provides the driving force for two components to phase separation. In addition, the crystallization of IEICO-4F occurs during the device aging and forms largely isolated IEICO-4F-phases (**Figure 8b**). These two factors lead to a lack of percolation pathways for electron transport resulting in evident burn-in degradation. The way to improve stability is mainly focused on suppressing the crystallization of acceptor and maintains the pathways for electron transport. The third component $PC_{71}BM$ is hyper-miscible with PTB7-Th but only partly miscible with IEICO-4F (**Figure 8c**). Therefore, the $PC_{71}BM$ are inclined to stay in donor-rich phases to form the transport paths and a bit of $PC_{71}BM$ permeates into acceptor-rich phases to suppress the crystallization of IEICO-4F simultaneously (as illustrated in **Figure 8d**), indeed giving rise to the stability of devices with more than 90% of initial PCE even after storing for 90 days.

In general, the addition of the third component provides a simple method to effectively improve the pristine photovoltaic performance and suppress the degradation of devices driven by thermodynamics simultaneously. A preliminary selection guideline especially toward the device stability can be referenced for the χ parameters of components. Studies up to date indicate that the selection of the third component is strongly materials-dependent, and there remains far away from establishing a general rule for the selection of the third component. To gain deeper insight into the relationship between material selection, film morphology, and device performance in ternary blend systems, more systematic and fundamental research is required.

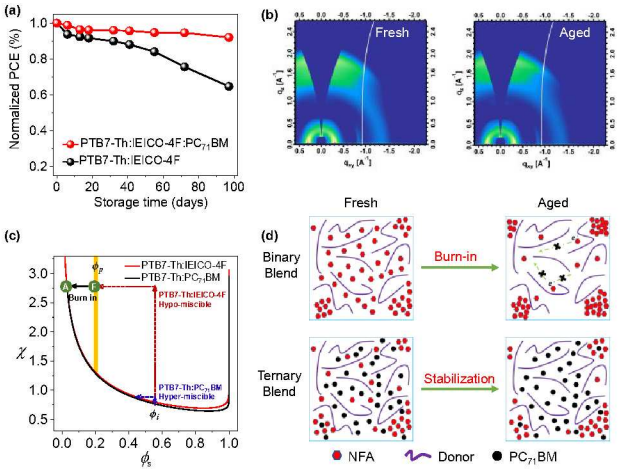

Figure 8. (a) *J-V* curves of PTB7-Th:IEICO-4F and PTB7-Th:IEICO-4F:$PC_{71}BM$ blend systems during aging in the dark. (b) Two-dimensional GIWAXS pattern for fresh and aged PTB7-Th:IEICO-4F blend films. (c) Schematic illustration of the χ-ϕ diagram for the PTB7-Th:IEICO-4F and PTB7-Th:$PC_{71}BM$ blends in relation to the electron transport percolation threshold. ϕ_s is the volume composition of the acceptor and ϕ_i indicates the initial volume composition of the acceptors as the D/A weight ratio of 1:1.5. Point F and point A represent the freshly prepared and aged film, respectively. (d) Schematic of morphology evolution of PTB7-Th:IEICO-4F system and PTB7-Th:IEICO-4F:$PC_{71}BM$ system during aging[110]. Reproduced with permission from ref. 109. Copyright 2019, John Wiley and Sons.

6. Role of Material:Solvent Interaction Parameter χ in PSCs

Beyond the material:material interaction discussed in prior sections, material:solvent interaction also plays a vital role in understanding the morphology development of PSC films[67, 112, 113]. It has been demonstrated that altering the material:solvent interactions in the solution prior to film-casting induces different solid-state morphological characteristics, which subsequently leads to different performances in PSCs[9, 114, 115]. In this section, we will use two case studies to showcase the potential of using material:solvent interaction parameter χ in understanding the morphology of PSCs and possibly guiding the device optimization.

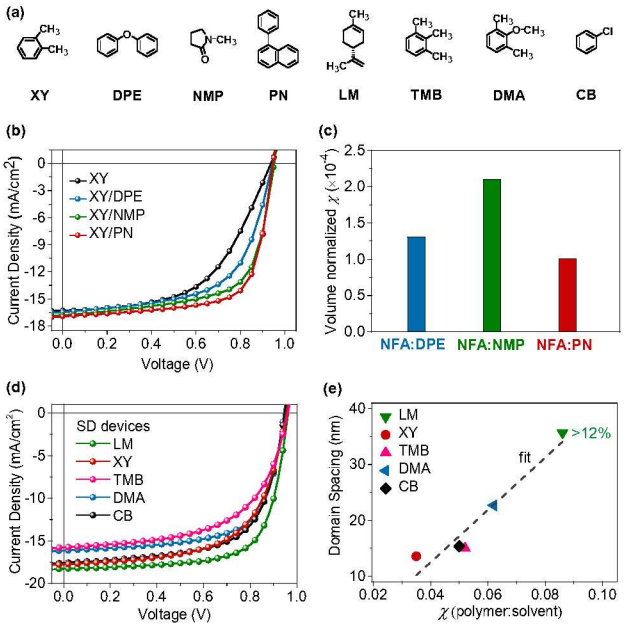

Figure 9. (a) Chemical structures of processing solvents and solvent additives used for fabricating PSCs devices. (b) Typical *J-V* curves of PBDB-T:IT-M based bulk-heterojunction PSC devices fabricated with different halogen-free solvent systems[116]. Reproduced with permission from ref. 115. Copyright 2017, Springer Nature. (c) Plot of volume normalized NFA:solvent interaction parameter χ. (d) Representative *J-V* curves of sequentially deposited PSC devices based on FTAZ/IT-M with different solvent systems. (e) Plot of domain spacing of the sequentially deposited PSCs and polymer:solvent interaction parameter χ[117]. Reprinted with permission from ref. 116. Copyright 2019, John Wiley and Sons.

The development of environmentally-benign solvents is a critical step to advancing the commercialization of PSCs[118-120]. Usually, solvent additives are introduced to finely tune the morphology of PSCs[113, 121, 122]. In the bulk-heterojunction devices of an important system PBDB-T:IT-M[123], incorporation of different halogen-free solvent additives such as N-methylpyrrolidone (NMP), diphenyl ether (DPE), and 1-phenylnaphthalene (PN) into the host solvent *o*-xylene (XY) results in notable differences in the device fill factors and power conversion efficiencies[116], as illustrated in **Figure 9a**. **Figure 9b** displays that PSC devices based on PN exhibited the highest *FF* of 72% and PCE of 11.6%. Starting from HSP, Zhao *et al.* estimated the volume normalized χ values of IT-M:DPE, IT-M:NMP, IT-M:PN pairs, which are 1.3×10^{-4}, 2.1×10^{-4}, 1.0×10^{-4}, respectively (as shown in **Figure 9c**). It is apparent that PN is a more favourable solvent additive for IT-M compared with DPE and NMP. As PN is more feasible with IT-M and exhibits a high boiling point, IT-M can form much more ordered packing and higher phase purity in the blend films, as confirmed by GIWAXS and R-SoXS results, respectively. Together, these results well explained the observed performance difference, implying a link between χ and PCE. As a consequence, screening environmentally-friendly solvent systems

for PSCs may be aided by the use of material:solvent interaction parameter χ.

To further demonstrate the role of processing solvent, the effect of processing solvent on neat polymer films requires in-depth studies. In our recent study, we demonstrated sequentially deposited PSCs based on a polymer donor PBnDT-FTAZ (also known as FTAZ) and a nonfullerene acceptor IT-M with eco-compatible solvents. Four different halogen-free solvents, namely, XY, toluene (TL), 1,2,4-trimethylbenzene (TMB), (R)-(+)-limonene (LM), and 2,6-dimethylanisole (DMA), were used to process FTAZ and the chlorinated solvent chlorobenzene (CB) was considered as a comparison. It was shown that the processing solvent of FTAZ has a profound influence on the domain spacing of the sequentially deposited nonfullerene PSCs[117]. The improved performance (**Figure 9d**) of FTAZ-based devices processed by R-limonene (LM) was closely associated with the highest χ parameter. Compared with other processing solvents, LM with the highest χ parameter of photoactive materials makes the film have more suitable domain spacing and highly ordered molecular arrangement through sequential deposition, in turn improving the device efficiency up to 12.5%. Applying this strategy, the sequentially deposited PSC devices outperform the bulk-heterojunction devices[124]. Notably, **Figure 9e** exhibits a monotonic (almost linear) relation between the domain spacing and polymer:solvent interaction parameter χ was observed. Although the origin of this relationship is not very clear and requires further investigations, the preliminary results demonstrated the great potential of applying material:solvent interaction parameters to optimize the PSC devices.

In the device preparation of PSCs, the selection of processing solvent plays an indispensable role. The boiling point of solvent is a commonly considered factor and closely related to the film-forming kinetics. Besides, the interaction parameters of material:solvent is the key factor affecting device performance from a thermodynamic perspective, which can be predicted by using HSPs. In some cases, higher interaction parameter χ is conducive to pre-aggregation of the material in solvent. The formation of molecular aggregates in solution prior to deposition of the film, resulting in pure domains with appropriate molecular packing structure, which leads to the higher *FF* and PCE[125]. On the other hand, pre-aggregation is related to nucleation dynamics, which also affects the domain size and phase purity of the film[126-128]. However, the specific analysis of this pre-aggregation aspect is beyond the scope of this article.

Concluding Remarks and Outlook

Summarizing, this Feature Article provided an overview of the most recent advances in the mixing thermodynamics of conjugated polymers and their applications in understanding nonfullerene PSCs, with a focus on those based on polymer donor and nonfullerene small molecule acceptor blends. Based on various types of high-efficiency polymer:nonfullerene composites, we have demonstrated how to realize high-performance PSCs from the viewpoint of mixing thermodynamics. In particular, the significance of interaction parameter χ in understanding the morphology of nonfullerene acceptors with two types of donor polymers (benzodithiophene-based polymers, polythiophene derivatives) and their device function (performance and stability) were discussed. It should be noted that blend films cast from solution are often kinetically trapped and likely in metastable state rather than thermodynamic equilibrium state even after post treatments[98]. To provide a comprehensive insight into the morphology manipulation, kinetic effects should be comprehensively considered. Despite the recent advances in these polymer:nonfullerene small molecule blends, many open questions related to thermodynamic interaction parameters still need to be addressed.

(1) **Temperature dependence of interaction parameters.** Currently, the temperature dependence of interaction parameter, *i.e.*, $\chi(T)$ has been only determined for a few PSC systems[61, 62]. To guide the selection of processing parameters (*e.g.*, post-treatment temperature), $\chi(T)$ should be more widely determined. Constructing a new database of conjugated polymer:molecule blends with experimentally determined χ parameters will offer some valuable lessons about device processing and importantly provide quantitative insights into the relationships between χ and other properties of basic physics processes (exciton diffusion, charge transport, *etc*).

(2) **Effect of molecular mass polydispersity.** Almost all the polymer is polydisperse, which is not taken into consideration by Flory-Huggins theory[129]. This is an unexplored problem in the field, as the preparation of a set of materials with polydispersity as the only variable is a grand challenge. To consider this factor, new models also need to be developed to understand the molecular weight polydispersity of PSC systems. It was shown that continuous thermodynamics models[130] are capable of describing this aspect. In principle, it would be possible to apply the model for PSCs based on polydisperse polymer blends.

(3) **Effect of crystalline-amorphous interactions.** The molecular interactions between two blend components are much more complex[131], which can not be only described with a single parameter, *i.e.*, amorphous-amorphous interaction parameter (χ_{aa}). Presently, amorphous-amorphous interaction parameter χ_{aa} was characterized and studied for many PSC systems, while in the semi-crystalline blend system, crystalline-amorphous and amorphous-crystalline interaction parameters, *i.e.*, χ_{ac} and χ_{ca} were only characterized in a few studies[61] based on a self-consistent model by Kyu and co-workers[47], and the relation between these interaction parameters and device performance remains poorly understood. To accounts for both amorphous-amorphous and crystalline-amorphous interactions in polymer blends containing crystalline components, χ_{ac} and χ_{ca} should be quantitatively and comprehensively analysed and correlated with film morphology and device function.

(4) **Extension to many other polymer:small blends.** Although the systems used in this article mainly comprised of a polymer donor and a nonfullerene small molecule acceptor, the relations of polymer donor:small molecule acceptor as parameterized with the theory of Flory and Huggins can be likely extended to other kinds of blends used in electronics such as small molecule donor/polymer acceptor blends[132] and conjugated polymer/volatilizable solid additive for solar cells, and polymer:small molecule blends for transistors as well as conjugated polymer/dopant blends for versatile applications in thermoelectrics, transistors, and solar cells. Most recent results by Han *et al.* have demonstrated that determining interaction parameters is instructive to understand these blends[133-135].

(5) **Characterization of χ for complex polymer systems.** Beyond polymer:small molecule blend systems, polymer donor:polymer acceptor blends[136-139] and double-cable polymers[140-142] are under active development and demonstrated great potentials in long-term stability. and impressive efficiency of 14.4% has been achieved in an all-polymer PSC device reported by Huang *et al*.[143] and a promising PCE of 8.4% has been realized in single component PSCs based on a double cable polymer developed by Li group.[56] Currently, the χ parameters of these polymer systems are still inadequately characterized, mostly by the contact angle method. New measures based on other methods might be useful to deduce the structure-performance relationships of these complex polymer blends.

(6) **Computational investigation of interaction parameters**. While our focus here has been on the experimental determination of χ, computer-aided simulations are ideal solutions to determine interaction parameters. Currently, efforts on simulating χ are much less compared with experimental investigations[144]. Since very rare cases have presented both simulated and experimentally determined χ, the computational results have to be compared and refined with experiments. To speed up the advances, more computational efforts are needed[145, 146]. For instance, a recent study by Zhang and co-workers[147] has introduced a new thermodynamic integration scheme to simulate χ parameters, which might be applicable to PSC systems.

Addressing the above challenges may vastly reduce the parameter space of the trial-and-error material synthesis and device optimization approaches by clearly eliminating a large number of material pairs and processing protocols. The establishment of more comprehensive χ-morphology-function relations would eventually enable predicting optimum processing parameters and material combinations for the manufacture of high-performance PSCs. Lastly, we hope to extend the above relations and methodologies of PSCs to understand polymer electronics such as light-emitting diodes, thin-film transistors, thermoelectrics, and photodetectors, where polymer blends are also widely used as the active layers.

Conflicts of interest

There are no conflicts to declare.

Acknowledgements

The Peiyang Scholar Program of Tianjin University and the Open Fund of State Key Laboratory of Luminescent Materials and Devices (South China University of Technology, 2020-skllmd-11) are appreciated for supporting the preparation of this paper. Some published case studies discussed in this work were supported by the U.S. Office of Naval Research (No. N000141712204) and the National Natural Science Foundation of China (Nos. 51703158 and 21774093). We gratefully acknowledge all the researchers who contributed to the advances and collaborators as appeared in the references. Especially, L. Ye would like to thank Prof. H. Ade (NCSU) for his fruitful discussion.

Author Biographies

Mengyuan Gao earned her Bachelor degree in polymer materials & engineering from Taiyuan University of Technology, China, in July 2019. Presently, she is a graduate student at the school of Materials Science & Engineering of Tianjin University under the supervision of Prof. Long Ye and Prof. Yanhou Geng. Her research work focuses on understanding the mixing behaviours of conjugated polymer blends used in polymer solar cells and other types of electronics by applying polymer physics knowledge.

Ziqi Liang is currently a Ph.D. Student at the school of Materials Science & Engineering of Tianjin University under the direction of Prof. Yanhou Geng. She obtained her Bachelor degree in polymer materials & engineering from Shandong University in July 2017. Her current research interests are designing and optimizing organic/polymeric materials for low cost nonfullerene solar cells.

Yanhou Geng is a full professor at the School of Materials Science and Engineering, Tianjin University, China. He received his PhD degree from Changchun Institute of Applied Chemistry (CIAC), Chinese Academy of Sciences in 1996. From 1998 to 2003, he worked in the Max Planck Institute for Polymer Research in Mainz (Germany) as an AvH stipendiat and the University of Rochester (USA) as a postdoctoral researcher. From 2003 to 2015, he was a professor at CIAC. His research interests include (1) polymerization methods for conjugated polymers; (2) organic and polymeric semiconductors for solar cells and thin-film transistors.

Long Ye is a Professor at the School of Materials Science & Engineering of Tianjin University since October 2019. He received his Ph.D. degree from Institute of Chemistry, Chinese Academy of Sciences (Adviser: Prof. Jianhui Hou) in July 2015. From August 2015 to September 2019, he was a postdoctoral researcher and later promoted to research assistant professor in the same group headed by Prof. Harald Ade at the Department of Physics, North Carolina State University. His current interests include morphological and mechanical characterizations of semiconducting polymers and their blends in solar cells and transistors, and polymer physics of conjugated polymers.

Notes and references

1. Y. Cui, Y. Wang, J. Bergqvist, H. Yao, Y. Xu, B. Gao, C. Yang, S. Zhang, O. Inganäs, F. Gao and J. Hou, *Nat. Energy*, 2019, **4**, 768-775.
2. C. Sun, R. Xia, H. Shi, H. Yao, X. Liu, J. Hou, F. Huang, H.-L. Yip and Y. Cao, *Joule*, 2018, **2**, 1816-1826.
3. C. J. M. Emmott, J. A. Röhr, M. Campoy-Quiles, T. Kirchartz, A. Urbina, N. J. Ekins-Daukes and J. Nelson, *Energy Environ. Sci.*, 2015, **8**, 1317-1328.
4. N. C. Davy, M. Sezen-Edmonds, J. Gao, X. Lin, A. Liu, N. Yao, A. Kahn and Y.-L. Loo, *Nat. Energy*, 2017, **2**, 17104.
5. L. K. Reb, M. Böhmer, B. Predeschly, S. Grott, C. L. Weindl, G. I. Ivandekic, R. Guo, C. Dreißigacker, R. Gernhäuser, A. Meyer and P. Müller-Buschbaum, *Joule*, 2020, DOI: https://doi.org/10.1016/j.joule.2020.07.004.
6. K. Wang, K. Amin, Z. An, Z. Cai, H. Chen, H. Chen, Y. Dong, X. Feng, W. Fu, J. Gu, Y. Han, D. Hu, R. Hu, D. Huang, F. Huang, F. Huang, Y. Huang, J. Jin, X. Jin, Q. Li, T. Li, Z. Li, Z. Li, J. Liu, J. Liu, S. Liu, H. Peng, A. Qin, X. Qing, Y. Shen, J. Shi, X. Sun, B. Tong, B. Wang, H. Wang, L. Wang, S. Wang, Z. Wei, T. Xie, C. Xu, H. Xu, Z.-K. Xu, B. Yang, Y. Yu, X. Zeng, X. Zhan, G. Zhang, J. Zhang, M. Q. Zhang, X.-Z. Zhang, X. Zhang, Y. Zhang, Y. Zhang, C. Zhao, W. Zhao, Y. Zhou, Z. Zhou, J. Zhu, X. Zhu and B. Z. Tang, *Mater. Chem. Front.*, 2020, **4**, 1803-1915.
7. F. Huang, Z. Bo, Y. Geng, X. Wang, L. Wang, Y. Ma, J. Hou, W. Hu, J. Pei, H. Dong, S. Wang, Z. Li, Z. Shuai, Y. Li and Y. Cao, *Acta Polym. Sin.*, 2019, **50**, 988-1046.
8. K. Gao, W. Deng, L. Xiao, Q. Hu, Y. Kan, X. Chen, C. Wang, F. Huang, J. Peng, H. Wu, X. Peng, Y. Cao, T. Russell and F. Liu, *Nano Energy*, 2016, **30**, 639-648.
9. L. Ye, S. Zhang, W. Ma, B. Fan, X. Guo, Y. Huang, H. Ade and J. Hou, *Adv. Mater.*, 2012, **24**, 6335-6341.
10. H. Lee, C. Park, D. H. Sin, J. H. Park and K. Cho, *Adv. Mater.*, 2018, **30**, 1800453.
11. X. Liu, C. Zhang, C. Duan, M. Li, Z. Hu, J. Wang, F. Liu, N. Li, C. J. Brabec, R. A. J. Janssen, G. C. Bazan, F. Huang and Y. Cao, *J. Am. Chem. Soc.*, 2018, **140**, 8934-8943.
12. Z. Hamid, A. Wadsworth, E. Rezasoltani, S. Holliday, M. Azzouzi, M. Neophytou, A. A. Y. Guilbert, Y. Dong, M. S. Little, S. Mukherjee, A. A. Herzing, H. Bristow, R. J. Kline, D. M. DeLongchamp, A. A. Bakulin, J. R. Durrant, J. Nelson and I. McCulloch, *Adv. Energy Mater.*, 2020, **10**, 1903248.
13. Q. Liu, Y. Jiang, K. Jin, J. Qin, J. Xu, W. Li, J. Xiong, J. Liu, Z. Xiao, K. Sun, S. Yang, X. Zhang and L. Ding, *Sci. Bull.*, 2020, **65**, 272-275.
14. L. Meng, Y. Zhang, X. Wan, C. Li, X. Zhang, Y. Wang, X. Ke, Z. Xiao, L. Ding, R. Xia, H. L. Yip, Y. Cao and Y. Chen, *Science*, 2018, **361**, 1094-1098.
15. A. Levitsky, G. M. Matrone, A. Khirbat, I. Bargigia, X. Chu, O. Nahor, T. Segal-Peretz, A. J. Moulé, L. J. Richter, C. Silva, N. Stingelin and G. L. Frey, *Adv Sci*, 2020, **7**, 2000960.
16. J. Zhang, H. Tan, X. Guo, A. Facchetti and H. Yan, *Nat. Energy*, 2018, **3**, 720-731.
17. B. Cao, L. A. Adutwum, A. O. Oliynyk, E. J. Luber, B. C. Olsen, A. Mar and J. M. Buriak, *ACS Nano*, 2018, **12**, 7434-7444.
18. B. Watts, W. J. Belcher, L. Thomsen, H. Ade and P. C. Dastoor, *Macromolecules*, 2009, **42**, 8392-8397.
19. B. A. Collins, E. Gann, L. Guignard, X. He, C. R. McNeill and H. Ade, *J. Phys. Chem. Lett.*, 2010, **1**, 3160-3166.
20. N. D. Treat, M. A. Brady, G. Smith, M. F. Toney, E. J.

Kramer, C. J. Hawker and M. L. Chabinyc, *Adv. Energy Mater.*, 2011, **1**, 82-89.
21. D. Chen, F. Liu, C. Wang, A. Nakahara and T. P. Russell, *Nano Lett.*, 2011, **11**, 2071-2078.
22. N. D. Treat, A. Varotto, C. J. Takacs, N. Batara, M. Al-Hashimi, M. J. Heeney, A. J. Heeger, F. Wudl, C. J. Hawker and M. L. Chabinyc, *J. Am. Chem. Soc.*, 2012, **134**, 15869-15879.
23. K. Vakhshouri, D. Kozub, C. Wang, A. Salleo and E. Gomez, *Phys. Rev. Lett.*, 2012, **108**, 026601.
24. B. A. Collins, Z. Li, C. R. McNeill and H. Ade, *Macromolecules*, 2011, **44**, 9747-9751.
25. W. Ma, J. R. Tumbleston, M. Wang, E. Gann, F. Huang and H. Ade, *Adv. Energy Mater.*, 2013, **3**, 864-872.
26. J. R. Tumbleston, A. C. Stuart, E. Gann, W. You and H. Ade, *Adv. Funct. Mater.*, 2013, **23**, 3463-3470.
27. B. A. Collins, Z. Li, J. R. Tumbleston, E. Gann, C. R. McNeill and H. Ade, *Adv. Energy Mater.*, 2013, **3**, 65-74.
28. W. Ma, J. R. Tumbleston, L. Ye, C. Wang, J. Hou and H. Ade, *Adv. Mater.*, 2014, **26**, 4234-4241.
29. H. Chen, J. Peet, S. Hu, J. Azoulay, G. Bazan and M. Dadmun, *Adv. Funct. Mater.*, 2014, **24**, 140-150.
30. B. A. Collins, J. R. Tumbleston and H. Ade, *J. Phys. Chem. Lett.*, 2011, **2**, 3135-3145.
31. J. Song, M. Zhang, M. Yuan, Y. Qian, Y. Sun and F. Liu, *Small Methods*, 2018, **2**, 1700229.
32. L. Ye, B. A. Collins, X. Jiao, J. Zhao, H. Yan and H. Ade, *Adv. Energy Mater.*, 2018, **8**, 1870124.
33. P. Knychała, K. Timachova, M. Banaszak and N. P. Balsara, *Macromolecules*, 2017, **50**, 3051-3065.
34. F. Bates, *Science*, 1991, **251**, 898.
35. P. J. Flory, *Principles of Polymer Chemistry*, Cornell University Press, 1953.
36. N. D. Treat, P. Westacott and N. Stingelin, *Annu. Rev. Mater. Res.*, 2015, **45**, 459-490.
37. P. Westacott, N. D. Treat, J. Martin, J. H. Bannock, J. C. de Mello, M. Chabinyc, A. B. Sieval, J. J. Michels and N. Stingelin, *Journal of Materials Chemistry A*, 2017, **5**, 2689-2700.
38. C. Schaefer, J. J. Michels and P. van der Schoot, *Macromolecules*, 2017, **50**, 5914-5919.
39. C. Schaefer, J. J. Michels and P. van der Schoot, *Macromolecules*, 2016, **49**, 6858-6870.
40. J. J. Michels and E. Moons, *Macromolecules*, 2013, **46**, 8693-8701.
41. M. Kim, J. Lee, S. B. Jo, D. H. Sin, H. Ko, H. Lee, S. G. Lee and K. Cho, *J. Mater. Chem. A*, 2016, **4**, 15522-15535.
42. S. Kouijzer, J. J. Michels, M. van den Berg, V. S. Gevaerts, M. Turbiez, M. M. Wienk and R. A. J. Janssen, *J. Am. Chem. Soc.*, 2013, **135**, 12057-12067.
43. F. Liu, D. Chen, C. Wang, K. Luo, W. Gu, A. L. Briseno, J. W. P. Hsu and T. P. Russell, *ACS Appl. Mater. Interfaces*, 2014, **6**, 19876-19887.
44. J. Y. Kim, *Macromolecules*, 2019, **52**, 4317-4328.
45. J. D. Perea, S. Langner, M. Salvador, B. Sanchez-Lengeling, N. Li, C. Zhang, G. Jarvas, J. Kontos, A. Dallos, A. Aspuru-Guzik and C. J. Brabec, *J. Phys. Chem. C*, 2017, **121**, 18153-18161.
46. D. M. Stoltzfus, A. J. Clulow, H. Jin, P. L. Burn and I. R. Gentle, *Macromolecules*, 2016, **49**, 4404-4415.
47. R. Matkar and T. Kyu, *J. Phys. Chem. B*, 2006, **110**, 12728-12732.
48. R. Matkar and T. Kyu, *J. Phys. Chem. B*, 2006, **110**, 16059-16065.
49. T. P. Russell, R. P. Hjelm and P. A. Seeger, *Macromolecules*, 1990, **23**, 890-893.
50. Z. Peng, X. Jiao, L. Ye, S. Li, J. Rech, W. You, J. Hou and H. Ade, *Chem. Mater.*, 2018, **30**, 3943-3951.
51. T. Nishi and T. T. Wang, *Macromolecules*, 1975, **8**, 909-915.
52. D. R. Kozub, K. Vakhshouri, L. M. Orme, C. Wang, A. Hexemer and E. D. Gomez, *Macromolecules*, 2011, **44**, 5722-5726.
53. Z. Liang, M. Li, Q. Wang, Y. Qin, S. J. Stuard, Z. Peng, Y. Deng, H. Ade, L. Ye and Y. Geng, *Joule*, 2020, **4**, 1278-1295.
54. Q. Wang, M. Li, X. Zhang, Y. Qin, J. Wang, J. Zhang, J. Hou, R. A. J. Janssen and Y. Geng, *Macromolecules*, 2019, **52**, 4464-4474.
55. Q. Wang, Z. Hu, Z. Wu, Y. Lin, L. Zhang, L. Liu, Y. Ma, Y. Cao and J. Chen, *ACS Appl. Mater. Interfaces*, 2020, **12**, 4659-4672.
56. X. Jiang, J. Yang, S. Karuthedath, J. Li, W. Lai, C. Li, C. Xiao, L. Ye, Z. Ma, Z. Tang, F. Laquai and W. Li, *Angew. Chemie. Int. Ed.*, 2020, DOI: 10.1002/anie.202009272
57. W. Li, L. Ye, S. Li, H. Yao, H. Ade and J. Hou, *Adv. Mater.*, 2018, **30**, 1707170.
58. Q. Guo, J. Lin, H. Liu, X. Dong, X. Guo, L. Ye, Z. Ma, Z. Tang, H. Ade, M. Zhang and Y. Li, *Nano Energy*, 2020, **74**, 104861.
59. S. Li, L. Ye, W. Zhao, H. Yan, B. Yang, D. Liu, W. Li, H. Ade and J. Hou, *J. Am. Chem. Soc.*, 2018, **140**, 7159-7167.
60. D. Yuan, F. Pan, L. Zhang, H. Jiang, M. Chen, W. Tang, G. Qin, Y. Cao and J. Chen, *Solar RRL*, 2020, **4**, 2000062.
61. L. Ye, H. Hu, M. Ghasemi, T. Wang, B. A. Collins, J.-H. Kim, K. Jiang, J. H. Carpenter, H. Li, Z. Li, T. McAfee, J. Zhao, X. Chen, J. L. Y. Lai, T. Ma, J.-L. Bredas, H. Yan and H. Ade, *Nat. Mater.*, 2018, **17**, 253-260.
62. M. Ghasemi, H. Hu, Z. Peng, J. J. Rech, I. Angunawela, J. H. Carpenter, S. J. Stuard, A. Wadsworth, I. McCulloch, W. You and H. Ade, *Joule*, 2019, **3**, 1328-1348.
63. Y. C. Bae, S. M. Lambert, D. S. Soane and J. M. Prausnitz, *Macromolecules*, 1991, **24**, 4403-4407.
64. B. Kuei and E. D. Gomez, *Soft Matter*, 2016, **13**, 49-67.
65. E. L. Hynes, J. T. Cabral, A. J. Parnell, P. Gutfreund, R. J. L. Welbourn, A. D. F. Dunbar, D. Môn and A. M. Higgins, *Commun. Phys.*, 2019, **2**, 112.
66. J. A. Emerson, D. T. W. Toolan, J. R. Howse, E. M. Furst and T. H. Epps, *Macromolecules*, 2013, **46**, 6533-6540.
67. Q. Zhang, Z. Y. Chen, W. Ma, Z. Y. Xie, J. G. Liu, X. H. Yu and Y. C. Han, *ACS Appl. Mater. Interfaces*, 2019, **11**, 32200-32208.
68. D. Leman, M. Kelly, S. Ness, S. Engmann, A. Herzing, C. Snyder, H. Ro, R. Kline, D. DeLongchamp and L. Richter, *Macromolecules*, 2015, **48**, 383-392.
69. M. Ghasemi, L. Ye, Q. Zhang, L. Yan, J. Kim, O. Awartani, W. You, A. Gadisa and H. Ade, *Adv. Mater.*, 2017, **29**, 1604603.
70. L. Ye, B. Collins, X. Jiao, J. Zhao, H. Yan and H. Ade, *Adv. Energy Mater.*, 2018, **8**, 1703058.
71. D. T. Duong, B. Walker, J. Lin, C. Kim, J. Love, B. Purushothaman, J. E. Anthony and T.-Q. Nguyen, *J. Poly. Sci. Part B: Polym. Phys.*, 2012, **50**, 1405-1413.
72. F. Machui, S. Abbott, D. Waller, M. Koppe and C. J. Brabec, *Macromol. Chem. Phys.*, 2011, **212**, 2159-2165.
73. J. Rivnay, S. C. B. Mannsfeld, C. E. Miller, A. Salleo and M. F. Toney, *Chem. Rev.*, 2012, **112**, 5488-5519.
74. X. Jiao, L. Ye and H. Ade, *Adv. Energy Mater.*, 2017, **7**, 1700084.

75. L. Ye, S. Stuard and H. Ade, in *Conjugated Polymers: Properties, Processing, and Applications*, eds. J. R. Reynolds, B. C. Thompson and T. A. Skotheim, CRC Press, 2019, DOI: DOI: 10.1201/9780429190520-13, ch. 13.
76. F. Liu, M. A. Brady and C. Wang, *Eur. Polym. J.*, 2016, **81**, 555-568.
77. B. P. Lyons, N. Clarke and C. Groves, *Energy Environ. Sci.*, 2012, **5**, 7657-7663.
78. L. Ye, S. Li, X. Liu, S. Zhang, M. Ghasemi, Y. Xiong, J. Hou and H. Ade, *Joule*, 2019, **3**, 443-458.
79. Y. Liu, J. Zhao, Z. Li, C. Mu, W. Ma, H. Hu, K. Jiang, H. Lin, H. Ade and H. Yan, *Nat. Commun.*, 2014, **5**, 5293.
80. S. Roland, M. Schubert, B. A. Collins, J. Kurpiers, Z. Chen, A. Facchetti, H. Ade and D. Neher, *J. Phys. Chem. Lett.*, 2014, **5**, 2815-2822.
81. S. Mukherjee, C. M. Proctor, G. C. Bazan, T. Q. Nguyen and H. Ade, *Adv. Energy Mater.*, 2015, **5**, 1500877.
82. L. Ye, X. Jiao, S. Zhang, H. Yao, Y. Qin, H. Ade and J. Hou, *Adv. Energy Mater.*, 2017, **7**, 1601138.
83. B. Zhang, Y. G. Yu, J. D. Zhou, Z. F. Wang, H. R. Tang, S. K. Xie, Z. Q. Xie, L. Y. Hu, H. L. Yip, L. Ye, H. Ade, Z. T. Liu, Z. C. He, C. H. Duan, F. Huang and Y. Cao, *Adv. Energy Mater.*, 2020, **10**, 1904247.
84. C. Yang, S. Zhang, J. Ren, M. Gao, P. Bi, L. Ye and J. Hou, *Energy Environ. Sci.*, 2020, DOI: 10.1039/D0EE01763A.
85. L. Ye, W. Zhao, S. Li, S. Mukherjee, J. Carpenter, O. Awartani, X. Jiao, J. Hou and H. Ade, *Adv. Energy Mater.*, 2017, **7**, 1602000.
86. L. Ye, W. Li, X. Guo, M. Zhang and H. Ade, *Chem. Mater.*, 2019, **31**, 6568-6577.
87. J. Xiao, M. Ren, G. Zhang, J. Wang, D. Zhang, L. Liu, N. Li, C. Brabec, H. Yip and Y. Cao, *Solar RRL*, 2019, **3**, 1900077.
88. J. A. Bartelt, Z. M. Beiley, E. T. Hoke, W. R. Mateker, J. D. Douglas, B. A. Collins, J. R. Tumbleston, K. R. Graham, A. Amassian, H. Ade, J. M. J. Fréchet, M. F. Toney and M. D. McGehee, *Adv. Energy Mater.*, 2013, **3**, 364-374.
89. Q. Fan, W. Su, Y. Wang, B. Guo, Y. Jiang, X. Guo, F. Liu, T. P. Russell, M. Zhang and Y. Li, *Sci. China Chem.*, 2018, **61**, 531-537.
90. J. Fang, Q. Liu, J. Zhang, L. Ye, J. Wu, Z. Wei, X. Guo, M. Zhang and Y. Li, *Solar RRL*, 2020, DOI: 10.1002/solr.202000275.
91. D. Baran, N. Gasparini, A. Wadsworth, C. H. Tan, N. Wehbe, X. Song, Z. Hamid, W. Zhang, M. Neophytou, T. Kirchartz, C. J. Brabec, J. R. Durrant and I. McCulloch, *Nat. Commun.*, 2018, **9**, 2059.
92. Y. Yan, X. Liu and T. Wang, *Adv. Mater.*, 2017, **29**, 1601674.
93. S. He, Z. Shen, J. Yu, H. Guan, G. Lu, T. Xiao, S. Yang, Y. Zou and L. Bu, *Adv. Mater. Interfaces*, 2020, DOI: 10.1002/admi.202000577.
94. Q. Li, L.-M. Wang, S. Liu, X. Zhan, T. Zhu, Z. Cao, H. Lai, J. Zhao, Y. Cai, W. Xie and F. Huang, *ACS Appl. Mater. Interfaces*, 2019, **11**, 45979-45990.
95. L.-M. Wang, Q. Li, S. Liu, Z. Cao, Y.-P. Cai, X. Jiao, H. Lai, W. Xie, X. Zhan and T. Zhu, *ACS Appl. Mater. Interfaces*, 2020, **12**, 24165-24173.
96. Z. Zhou, S. Xu, J. Song, Y. Jin, Q. Yue, Y. Qian, F. Liu, F. Zhang and X. Zhu, *Nat. Energy*, 2018, **3**, 952-959.
97. D. Baran, R. Ashraf, D. Hanifi, M. Abdelsamie, N. Gasparini, J. Rohr, S. Holliday, A. Wadsworth, S. Lockett, M. Neophytou, C. Emmott, J. Nelson, C. Brabec, A. Amassian, A. Salleo, T. Kirchartz, J. Durrant and I. McCulloch, *Nat. Mater.*, 2017, **16**, 363-369.
98. N. Yi, Q. Ai, W. Zhou, L. Huang, L. Zhang, Z. Xing, X. Li, J. Zeng and Y. Chen, *Chem. Mater.*, 2019, **31**, 10211-10224.
99. W. Zhong, J. Cui, B. Fan, L. Ying, Y. Wang, X. Wang, G. Zhang, X.-F. Jiang, F. Huang and Y. Cao, *Chem. Mater.*, 2017, **29**, 8177-8186.
100. R. Yu, H. Yao, Y. Cui, L. Hong, C. He and J. Hou, *Adv. Mater.*, 2019, **31**, 1902302.
101. K. Jiang, Q. Wei, J. Y. L. Lai, Z. Peng, H. K. Kim, J. Yuan, L. Ye, H. Ade, Y. Zou and H. Yan, *Joule*, 2019, **3**, 3020-3033.
102. H. Lu, J. Zhang, J. Chen, Q. Liu, X. Gong, S. Feng, X. Xu, W. Ma and Z. Bo, *Adv. Mater.*, 2016, **28**, 9559-9566.
103. K. Jiang, G. Zhang, G. Yang, J. Zhang, Z. Li, T. Ma, H. Hu, W. Ma, H. Ade and H. Yan, *Adv. Energy Mater.*, 2018, **8**, 1701370.
104. X. Ma, J. Wang, J. Gao, Z. Hu, C. Xu, X. Zhang and F. Zhang, *Adv. Energy Mater.*, 2020, **10**, 2001404.
105. H. B. Naveed and W. Ma, *Joule*, 2018, **2**, 621-641.
106. M. Ghasemi, L. Ye, Q. Zhang, L. Yan, J.-H. Kim, O. Awartani, W. You, A. Gadisa and H. Ade, *Adv. Mater.*, 2017, **29**, 1604603.
107. L. Zhang, N. Yi, W. Zhou, Z. Yu, F. Liu and Y. Chen, *Adv Sci*, 2019, **6**, 1900565.
108. M. Jørgensen, K. Norrman, S. A. Gevorgyan, T. Tromholt, B. Andreasen and F. C. Krebs, *Adv. Mater.*, 2012, **24**, 580-612.
109. L. Derue, O. Dautel, A. Tournebize, M. Drees, H. Pan, S. Berthumeyrie, B. Pavageau, E. Cloutet, S. Chambon, L. Hirsch, A. Rivaton, P. Hudhomme, A. Facchetti and G. Wantz, *Adv. Mater.*, 2014, **26**, 5831-5838.
110. Y. Zhu, A. Gadisa, Z. Peng, M. Ghasemi, L. Ye, Z. Xu, S. Zhao and H. Ade, *Adv. Energy Mater*, 2019, **9**, 1900376.
111. X. Song, N. Gasparini, L. Ye, H. Yao, J. Hou, H. Ade and D. Baran, *ACS Energy Lett.*, 2018, **3**, 669-676.
112. E. Pavlopoulou, C. S. Kim, S. S. Lee, Z. H. Chen, A. Facchetti, M. F. Toney and Y. L. Loo, *Chem. Mater.*, 2014, **26**, 5020-5027.
113. L. Ye, Y. Xiong, S. S. Li, M. Ghasemi, N. Balar, J. Turner, A. Gadisa, J. H. Hou, B. T. O'Connor and H. Ade, *Adv. Funct. Mater.*, 2017, **27**, 1702016.
114. F. Liu, W. Zhao, J. R. Tumbleston, C. Wang, Y. Gu, D. Wang, A. L. Briseno, H. Ade and T. P. Russell, *Adv. Energy Mater.*, 2014, **4**, 1301377.
115. J. Zhao, Y. Li, G. Yang, K. Jiang, H. Lin, H. Ade, W. Ma and H. Yan, *Nat Energy*, 2016, **1**, 15027.
116. W. Zhao, L. Ye, S. Li, X. Liu, S. Zhang, Y. Zhang, M. Ghasemi, C. He, H. Ade and J. Hou, *Sci. China Mater.*, 2017, **60**, 697-706.
117. L. Ye, Y. Xiong, Z. Chen, Q. Zhang, Z. Fei, R. Henry, M. Heeney, B. O'Connor, W. You and H. Ade, *Adv. Mater.*, 2019, **31**, 1808153.
118. S. Zhang, L. Ye, H. Zhang and J. Hou, *Mater. Today*, 2016, **19**, 533-543.
119. L. Ye, Y. Xiong, H. Yao, A. Gadisa, H. Zhang, S. Li, M. Ghasemi, N. Balar, A. Hunt, B. T. O'Connor, J. Hou and H. Ade, *Chem. Mater.*, 2016, **28**, 7451-7458.
120. Y. P. Qin, L. Ye, S. Q. Zhang, J. Zhu, B. Yang, H. Ade and J. H. Hou, *J. Mater. Chem. A*, 2018, **6**, 4324-4330.
121. C. McDowell, M. Abdelsamie, M. F. Toney and G. C. Bazan, *Adv. Mater.*, 2018, **30**, 1707114.
122. L. Ye, X. Jiao, W. Zhao, S. Zhang, H. Yao, S. Li, H. Ade and J. Hou, *Chem. Mater.*, 2016, **28**, 6178-6185.

123. S. Li, L. Ye, W. Zhao, S. Zhang, S. Mukherjee, H. Ade and J. Hou, *Adv. Mater.*, 2016, **28**, 9423-9429.
124. L. Ye, Y. Xiong, Q. Zhang, S. Li, C. Wang, Z. Jiang, J. Hou, W. You and H. Ade, *Adv. Mater.*, 2018, **30**, 1705485.
125. B. Xie, K. Zhang, Z. Hu, H. Fang, B. Lin, Q. Yin, B. He, S. Dong, L. Ying, W. Ma, F. Huang, H. Yan and Y. Cao, *Solar RRL*, 2020, **4**, 1900385.
126. Q. Zhang, Z. Chen, W. Ma, Z. Xie and Y. Han, *J. Mater. Chem. C*, 2019, **7**, 12560-12571.
127. J. J. van Franeker, M. Turbiez, W. Li, M. M. Wienk and R. A. J. Janssen, *Nat. Commun.*, 2015, **6**, 6229.
128. K. Zhou, J. Liu, M. Li, X. Yu, R. Xing and Y. Han, *J. Polym. Sci., Part B: Polym. Phys.*, 2015, **53**, 288-296.
129. Q. Chen, S. Xie, R. Foudazi, T. Lodge and J. Siepmann, *Macromolecules*, 2018, **51**, 3774-3787.
130. Y. Hu, X. Ying, D. T. Wu and J. M. Prausnitz, *Fluid Phase Equilib.*, 1995, **104**, 229-252.
131. S. S. Lee and Y.-L. Loo, *Annu. Rev. Chem. Biomol.*, 2010, **1**, 59-78.
132. Z. Zhang, J. Miao, Z. Ding, B. Kan, B. Lin, X. Wan, W. Ma, Y. Chen, X. Long, C. Dou, J. Zhang, J. Liu and L. Wang, *Nat. Commun.*, 2019, **10**, 3271.
133. R. Yu, H. Yao, L. Hong, M. Gao, L. Ye and J. Hou, *J. Mater. Chem. C*, 2020, **8**, 44-49.
134. Y. Tang, B. Lin, H. Zhao, T. Li, W. Ma and H. Yan, *ACS Appl. Mater. Interfaces*, 2020, **12**, 13021-13028.
135. Z. Chen, Y. Tang, B. Lin, H. Zhao, T. Li, T. Min, H. Yan and W. Ma, *ACS Appl. Mater. Interfaces*, 2020, **12**, 25115-25124.
136. H. Yin, C. Yan, H. Hu, J. K. W. Ho, X. Zhan, G. Li and S. K. So, *Mater. Sci. Eng. R Rep.*, 2020, **140**, 100542.
137. L. Ye, X. Jiao, M. Zhou, S. Zhang, H. Yao, W. Zhao, A. Xia, H. Ade and J. Hou, *Adv. Mater.*, 2015, **27**, 6046-6054.
138. G. Wang, F. S. Melkonyan, A. Facchetti and T. J. Marks, *Angew. Chem. Int. Ed.*, 2019, **58**, 4129-4142.
139. C. Lee, S. Lee, G. U. Kim, W. Lee and B. J. Kim, *Chem. Rev.*, 2019, **119**, 8028-8086.
140. J. Roncali and I. Grosu, *Adv Sci*, 2019, **6**, 1801026.
141. Y. He, T. Heumüller, W. Lai, G. Feng, A. Classen, X. Du, C. Liu, W. Li, N. Li and C. J. Brabec, *Adv. Energy Mater.*, 2019, **9**, 1900409.
142. G. Feng, J. Li, Y. He, W. Zheng, J. Wang, C. Li, Z. Tang, A. Osvet, N. Li, C. J. Brabec, Y. Yi, H. Yan and W. Li, *Joule*, 2019, **3**, 1765-1781.
143. T. Jia, J. Zhang, W. Zhong, Y. Liang, K. Zhang, S. Dong, L. Ying, F. Liu, X. Wang, F. Huang and Y. Cao, *Nano Energy*, 2020, **72**, 104718.
144. K. Do, C. Risko, J. E. Anthony, A. Amassian and J.-L. Brédas, *Chem. Mater.*, 2015, **27**, 7643-7651.
145. V. Coropceanu, X.-K. Chen, T. Wang, Z. Zheng and J.-L. Brédas, *Nat. Rev. Mater.*, 2019, **4**, 689-707.
146. T. Wang, G. Kupgan and J.-L. Brédas, *Trends in Chemistry*, 2020, **2**, 535-554.
147. W. Zhang, E. D. Gomez and S. T. Milner, *Phys. Rev. Lett.*, 2017, **119**, 017801.